Available online at www.sciencedirect.com
ScienceDirect
Nuclear Instruments and Methods in Physics Research A 579 (2007) 915–923
NUCLEAR INSTRUMENTS & METHODS IN PHYSICS RESEARCH Section A
www.elsevier.com/locate/nima

Double-negative metamaterial research for accelerator applications

S. Antipov[a], L. Spentzouris[a,*], W. Gai[b], W. Liu[b], J.G. Power[b]

[a]*Department of Biological, Chemical, and Physical Sciences, Illinois Institute of Technology, Chicago, IL 60616, USA*
[b]*Argonne National Laboratory, Argonne, IL 60439, USA*

Received 1 April 2007; received in revised form 14 April 2007; accepted 17 April 2007
Available online 1 May 2007

Abstract

Material properties are central to the design of particle accelerators. One area of advanced accelerator research is to investigate novel materials and structures and their potential use in extending capabilities of accelerator components. Within the past decade a new type of artificially constructed material having the unique property of simultaneously negative permittivity and permeability has been realized, and is under intense investigation, primarily by the optical physics and microwave engineering communities [C.M. Soukoulis, Science 315 (2007) 47; D.R. Smith, J.B. Pendry, M.C.K. Wiltshire, Science 305 (2004) 788; J.B. Pendry, A.J. Holden, W.J. Stewart, I. Youngs, Phys. Rev. Lett. 76 (1996) 4773]. Although they are typically constructed of arrays of discrete cells, as long as the condition that the wavelength of applied radiation is significantly greater than the cell dimensions is met, the material mimics a continuous medium and can be described with the bulk properties of permittivity, ε, and permeability, μ. When the permittivity and permeability are simultaneously negative in some frequency range, the metamaterial is called double negative (DNM) or left-handed (LHM) and has unusual properties, such as a negative index of refraction. An investigation of these materials in the context of accelerators is being carried out by IIT and the Argonne Wakefield Accelerator Facility [S. Antipov, W. Liu, W. Gai, J. Power, L. Spentzouris, AIP Conf. Proc. 877 (2006); S. Antipov, W. Liu, J. Power, L. Spentzouris, Design, Fabrication, and Testing of Left-Handed Metamaterial, Wakefield Notes at Argonne Wakefield Accelerator, ⟨http://www.hep.anl.gov/awa/wfnotes/wf229.pdf⟩]. Waveguides loaded with metamaterials are of interest because the DNM can change the dispersion relation of the waveguide significantly. For example, slow backward waves can be produced in a DNM-loaded waveguide without having corrugations. This article begins with a brief introduction of known design principles for realizing a DNM [J.B. Pendry, A.J. Holden, W.J. Stewart, I. Youngs, Phys. Rev. Lett. 76 (1996) 4773; D.R. Smith, et al., Phys. Rev. Lett. 84 (2000) 4184; J.B. Pendry, A.J. Holden, D.J. Robbins, W.J. Stewart, IEEE Trans. Microwave Theory Tech. 47 (1999) 2075], along with a description of the experimental verification of the basic DNM properties of our designs. We then present our waveguide analysis, starting with the case of a waveguide loaded with a truly continuous medium that is dispersive and anisotropic. We show that the dispersion relation of a waveguide with frequency regions of negative $\varepsilon(\omega)$ and negative $\mu(\omega)$ has several interesting frequency bands. While a DNM approximates a continuous medium, it is still made up of discrete elements. We discuss some implications of the discrete nature of the material for the behavior of a loaded waveguide, particularly at frequencies below the cutoff frequency of the waveguide. We conclude by describing our experimental program at present and in the near future. This includes testing the excitation of TM modes in a DNM loaded waveguide in the interesting frequency bands, both on the bench and from particle beam excitation.

PACS: 41.20.Jb; 41.60.Bq; 84.40.Az

Keywords: Loaded waveguide; Double-negative metamaterial; Wakefields; Dipole mode suppression

1. Introduction

In the present decade there has been intense interest in what are termed double-negative or left-handed metamaterials, because of their unusual response to applied radiation [1–3]. A metamaterial is a structure made of a repetitive array of unit cells. These are typically conducting strips and special loops with small gaps, called split-ring resonators, etched onto a substrate. When the physical dimensions of the cells are much smaller than the wavelength of applied radiation, the material can be

*Corresponding author. Tel.: +1 312 567 3577.
E-mail address: spentzouris@iit.edu (L. Spentzouris).

0168-9002/$ - see front matter © 2007 Elsevier B.V. All rights reserved.
doi:10.1016/j.nima.2007.04.158

described by the bulk properties permittivity, ε, and permeability, μ. If the permeability and permittivity are simultaneously negative in some frequency range, then a medium is termed double-negative, or left-handed. This combination of properties does not occur naturally. The electrodynamic behavior of Double-Negative Materials (DNM) was first investigated theoretically by Veselago [4]. Transmitted radiation has a phase velocity that counter-propagates with respect to the group velocity, and so obeys a left-handed rule for $\vec{E}$, $\vec{H}$, and $\vec{k}$, the electric, magnetic and phase vectors of the wave. The index of refraction, n, is negative in this circumstance. Pendry introduced principles for the design of DNMs in publications from 1996 [5] to 1999 [6]. This was followed by the construction of the first DNM by Smith et al. [7] in 2000.

Since the first realization of a DNM, there has been an explosion of research toward possible applications [1,3,8,9]. There is an intense research effort in the optical regime, stimulated by the possibility of ultrahigh-resolution imaging systems not offered with the current technology [1,3]. Due to the small cell size required in the optical range, development of the geometry and fabrication techniques is still an area of significant effort. In the microwave frequency range, achieving a DNM is less of a challenge, enabling a broad effort on microwave applications, such as the design of highly compact bandpass filters [8,9].

The behavior of materials has always played a central role in the design and construction of particle accelerators. An area of advanced accelerator research is to investigate novel methods, materials, or structures for their potential as high performance accelerator components, or for effectiveness in alleviating such problems as higher order mode excitation in accelerating structures. Notable work has been done at MIT on mode suppression through structure design, where a photonic band gap accelerating structure has been realized [10]. The MIT structure was a photonic crystal, a repetitive array of rods creating a frequency gap in which radiation cannot propagate through the structure. A defect in the array enables trapping of the accelerating mode. A group at the University of Texas [11] is working on surface wave accelerating SiC structures based on negative permittivity. Research efforts such as these use special geometries and materials to customize the response of a structure to electromagnetic excitation.

We report here on research being done at the Argonne Wakefield Accelerator facility [12–14]; specifically, an investigation of the use of DNM to control the dispersion relation in a loaded waveguide. Analysis done for a continuous anisotropic medium having the same permittivity and permeability tensors as a DNM shows synchronism between relativistic particles and the fundamental (backward) accelerating mode. It also shows a dipole mode below the cutoff frequency for the waveguide. Simulations have enabled a detailed study of the higher order modes of such a structure, assuming a continuous medium. Investigation is underway on how the discrete nature of the metamaterial affects these results. We have found that mode coupling in the structure depends on the relative placement of the split-ring resonators (SRRs) and the wire grids, as well as on the overall symmetry. Dipole mode suppression may depend on the discrete nature of the material in conjunction with being below the cutoff frequency of the waveguide. This is discussed, drawing on analysis of a waveguide loaded with a wire grid in what is termed the non-magnetic regime [15,16].

A description of our metamaterial designs, some discussion of the principles of DNMs, and some early experimental verification of the properties of our DNM are presented in Section 2. Section 3 has two parts, the first part gives analytic and simulation results for a waveguide loaded with a continuous, dispersive, anisotropic medium. The continuous medium is an approximation to our discrete-element structures. Our continuous media studies illuminate how the dispersion function of the loaded waveguide depends on the permittivity and permeability of the DNM design. The second part of Section 3 is devoted to discrete DNM structures. A discussion of potential dipole mode suppression is included, a feature that depends on the discrete nature of metamaterials. Section 5 concludes with a summary and the current status of our research.

2. Metamaterial design

Our double-negative metamaterial design follows the principles of the other earlier realized DNM designs [7,17]. It consists of either a wire array or an array of capacitively loaded strips for permittivity (ε) control, and an array of split-ring resonators for permeability (μ) control. These two arrays are put together as one continuous array of conducting strips and SRRs for simultaneous control of the permittivity and permeability. In order to obtain a double-negative metamaterial, there must be some frequency region in which both the permittivity and permeability are negative. If only one of these parameters is negative, electromagnetic waves will not be transmitted, the amplitude of the radiation will decay within the material. The permittivity and permeability must be simultaneously positive or simultaneously negative in order to have propagation through a material. Our first metamaterial design was done on a series of printed circuit boards, and is shown in Fig. 1. The middle of the three circuit boards of Fig. 1 has the capacitively loaded wire strips alone, the right-most of the three boards has only SRRs, and the left-most of the three boards has split-ring resonators and capacitively loaded strips combined.

2.1. Negative permittivity

Negative permittivity, ε, naturally occurs in plasmas at frequencies below the plasma frequency ω_p, and for conduction band electrons in metals at optical frequencies. A wire array can also exhibit plasma-like behavior in the

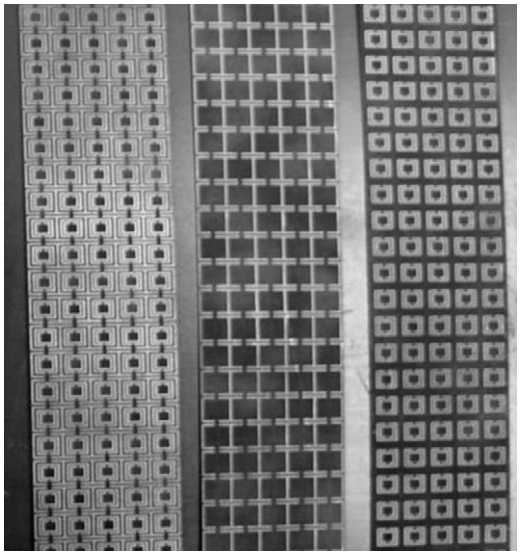

Fig. 1. Our first (anisotropic) metamaterial design. The leftmost board in the figure has split-ring resonators (SRR) and capacitively loaded strips (CLS) combined, the middle board has only CLS, and the right board has only SRR. A single cell (one split-ring resonator) is about 2.5 mm on a side. The resonant frequency of the SRRs for this design is about 11.5 GHz.

GHz frequency range [5,18,19] when the orientation of the applied electric field is along the wire direction. An analytical expression for the component of the permittivity tensor in the direction along the wires is given in Eq. (1), as stated in Ref. [5] (an antenna analysis as in Refs. [18,19] gives a similar result):

$$\varepsilon(\omega) = 1 - \frac{\omega_p^2}{\omega^2 + i\gamma\omega}$$
$$\omega_p^2 = \frac{2\pi c^2}{a^2 \ln(a/r)}$$
$$\gamma = \frac{c^2}{2\sigma S \ln(a/r)}. \quad (1)$$

In Eq. (1) and those that immediately follow, a is the periodic spacing between wires, r is the wire radius and S is the wire cross-section. A wire array such as shown in the center of Fig. 2 can produce plasma-like behavior (negative permittivity) only for electric fields that are parallel to the direction of the wires. Such a structure is anisotropic. In order to have an isotropic permittivity, the wires should be configured in a 3D grid such as is shown in the bottom right corner of Fig. 2. The dependence of the real and imaginary parts of ε on frequency are shown in Fig. 2. The permittivity, ε, is negative at frequencies below the plasma frequency. Capacitive bonds, such as those on the capacitively loaded strips shown in Fig. 1 are sometimes introduced into the conducting strips of a DNM to make the frequency dependence of ε resonant [13,17], similar to the frequency dependence of the permeability of split-ring resonators described next.

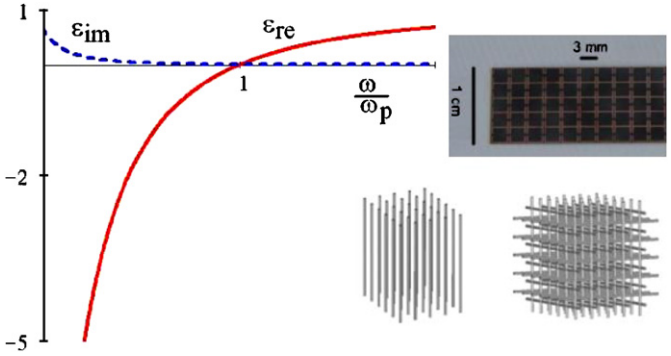

Fig. 2. The frequency dependence of the real and imaginary parts of the permittivity of a wire array. Frequency in the plot is normalized by the plasma frequency, ω_p, so the permittivity goes negative as the normalized frequency drops below one. The top-right inset shows capacitively loaded strips of our first design. The center inset shows a 1D wire array. The bottom-right inset shows a 3D wire array.

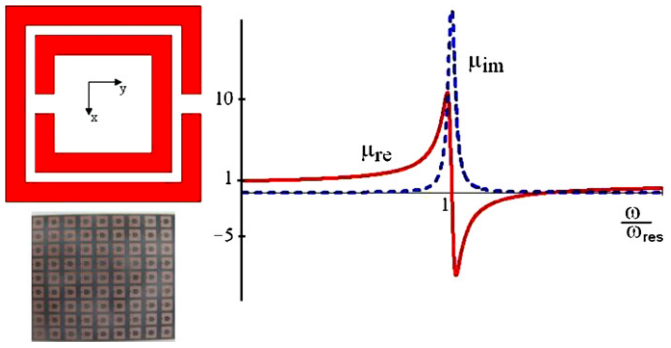

Fig. 3. The frequency dependence of the real and imaginary parts of the permeability of a split-ring resonator. Frequency in the plot is normalized by the resonant frequency, ω_{res}, so the permeability swings from positive to negative as the normalized frequency crosses one. A schematic and array of the split-ring resonators of our first design are also shown.

2.2. Negative permeability

Negative permeability in metamaterials is often realized via SRRs [6] for orientations where the applied magnetic field penetrates the plane of the loops (see Fig. 3). The cuts in the rings allow the resonant behavior, as they introduce a capacitance to the structure. Current loops are naturally inductive, and the introduced capacitance produces a resonant response in a frequency range that is dependent on the specific geometry of the rings. The design shown in Fig. 3 has two concentric split rings to increase the capacitive region and lower the resonance frequency. A typical frequency dependence for the permeability is also shown in Fig. 3. An analytical expression for the component of the permeability tensor in the direction perpendicular to the plane of the loops is given in Eq. (2), as stated in Ref. [6]:

$$\mu_{eff}(\omega) = 1 - \frac{F\omega^2}{\omega^2 - \omega_{res}^2 + i\gamma\omega}. \quad (2)$$

Here F is a geometrical factor. The resonant frequency, ω_{res}, and the loss factor, γ, are constants determined by

geometry and material properties. In the design, we studied at Argonne [12,13] we had a 2.54 mm overall size of the ring. The resonant frequency was designed to be 11.4 GHz ($\lambda \gg d$), and measurements verified that this was achieved.

Since the permeability is negative only for orientations where the magnetic field, $\vec{H}$, penetrates the plane of the rings, extra effort must be made to design an isotropic material. This can be done by arranging arrays of rings in different spatial orientations.

3. Experimental verification of double-negative properties

Two types of measurement were made to verify that we had realized a double-negative metamaterial. One of these was a direct measurement of the refraction angle of incident radiation to observe the effect of the negative index of refraction, n, using a method similar to that of Refs. [20,21]. A second measurement was of the transmitted and reflected power of incident radiation for a waveguide loaded with DNM, using the method of Ref. [22]. Both measurements verified that our metamaterial, an array of split-ring resonators and wires, exhibited double-negative behavior at the design frequency.

3.1. Measurement of refraction angle

When radiation passes from one medium, with index of refraction n_1, to another medium, with index of refraction n_2 (in this case air, $n_2 \sim 1$), the index of refraction of the medium is related to the angular deflection by Snell's law: $n_1 = \frac{\sin(\theta_2)}{\sin(\theta_1)}$. A negative index of refraction, n_1, causes the angle of transmitted radiation to be reversed with respect to the normal compared to the case of a positive index. Fig. 4 shows FDTD simulation results of transmission through a wedge of Teflon ($n = 1.42$) and through a double-negative medium ($n = -0.35$). The simulation of Fig. 4 shows a positive index of refraction for the Teflon wedge. There is a negative index of refraction for the double-negative medium, although a careful look is required, since the refracted radiation is close to the normal.

Experimental measurements of the refraction angle for a range of frequencies were performed for both Teflon and DNM wedges. A block diagram of our direct measurement of the index of refraction is shown in Fig. 5. Boards of the material were stacked into a wedge (with an air gap between boards). A network analyzer and a horn antenna were used to step the frequency of incident radiation on the wedge through the frequency range for double-negative behavior of the material. The position of the maximum of the transmitted radiation with respect to normal was determined using a movable probe for the range of applied frequencies. Both a Teflon wedge and a wedge of our metamaterial were tested. A plot of the extracted index of refraction versus frequency, based on the angular position of the maximum of the transmitted radiation, is shown for the Teflon wedge in Fig. 6(a) and for the metamaterial in Fig. 6(b).

The value of the index of refraction, n, obtained for the Teflon was within the manufacturer's specified range, as can be seen in Fig. 6(a). The value of n for the metamaterial swings negative around 11.7 GHz and returns to positive values around 12.4 GHz. The metamaterial is a DNM

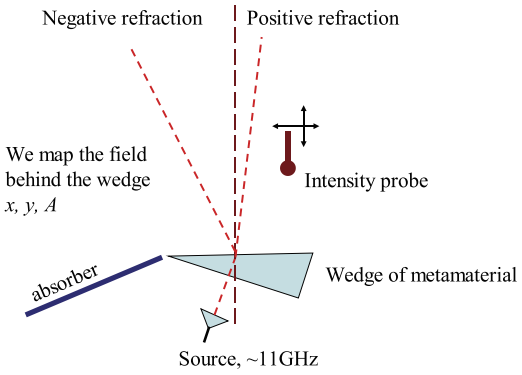

Fig. 5. Block diagram showing measurement of refraction angle of material. A network analyzer and horn antenna were used as the source of radiation. A movable probe on the other side of the wedge was used as a detector. The probe could move across the wedge as well as backward and forward. Received intensity versus probe position was used to obtain the angle of refraction.

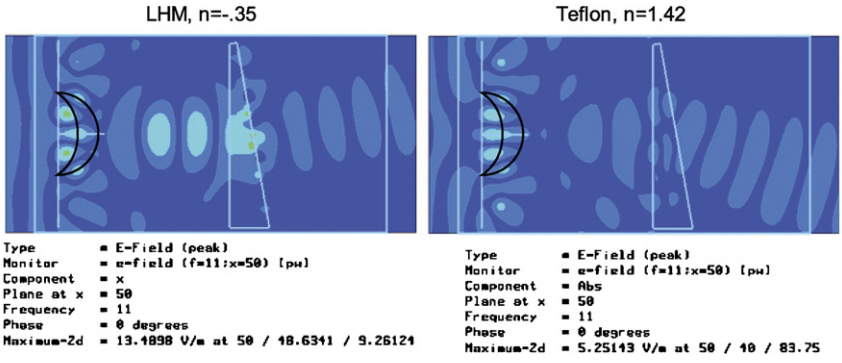

Fig. 4. Left: simulation of an electromagnetic wave transmitted through a wedge of DNM, with index of refraction, $n = -0.35$. Right: simulation of an electromagnetic wave transmitted through a wedge of Teflon material with index of refraction, $n = 1.42$.

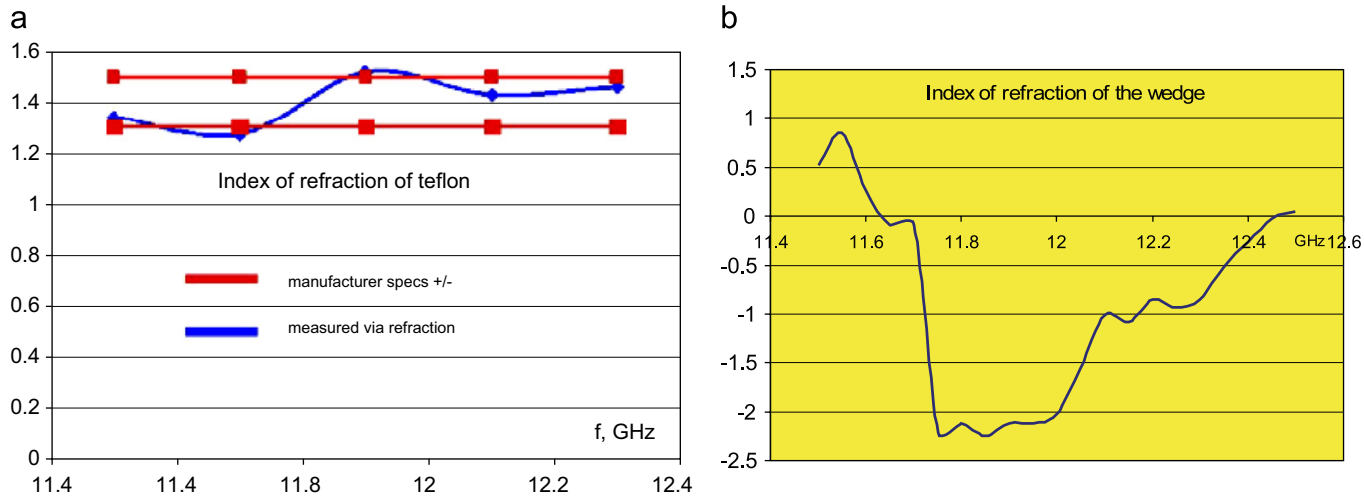

Fig. 6. Experimental results: index of refraction measurement. The left plot shows both the measured n for a wedge of Teflon and the range of the index of refraction for Teflon as specified by the manufacturer. The experimental values fall within the specifications. The right plot has the measured n for our wedge of DNM material; it switches from positive to negative and back around the resonant frequency of the split-ring resonators. (a) Teflon wedge, measured n (b) DNM wedge, measured n.

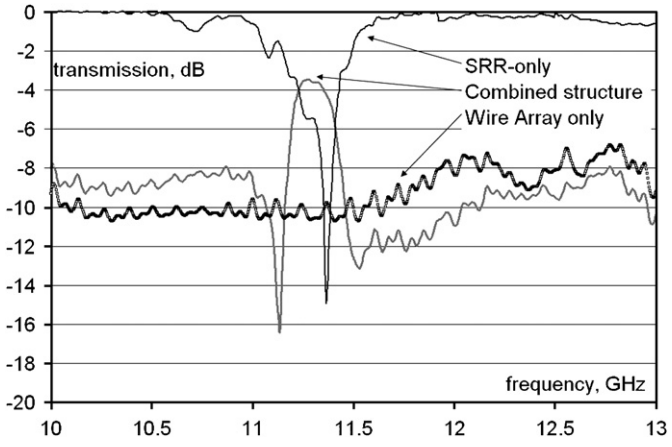

Fig. 7. Three measured transmission (S21) curves for TE_{10} from 10 to 13 GHz. Shown are the transmission curves for an array of split-ring resonators alone, a wire array alone, and for the split-ring resonators and wire array combined. There is a transmission peak for the combined structure in the region of overlap (double-negative region). (No effort was made to optimize transmission, this was a proof-of-principle measurement.)

around the design frequency, ω_{res}, and elsewhere has a positive index of refraction.

3.2. Transmission and reflection measurement

Transmission and reflection of incident radiation can be measured by doing an S21 and S11 measurement, respectively, using a network analyzer and two-port network. For this purpose, we loaded a waveguide with boards of our metamaterial and demonstrated the existence of a narrow double-negative band of propagation; the S21 results can be seen in Fig. 7. There are three TE_{10} transmission curves in this figure. The reasonably flat curve at ~10% transmission shows the result for the wire array alone. The curve with a strong dip in transmission at the resonant frequency (from 90% down to 10% near 11.4 GHz), shows the result for the SRRs alone. The curve showing a transmission peak at the resonant frequency of the SRRs (up to 40% transmission) shows the result for combined wire array and SRR array. The frequency range where the transmission through the SRRs drops precipitously is where the permeability of the structure goes negative. The wire array has a broad region of negative permittivity (all frequencies below ω_p) overlapping the range of negative permeability of the split rings. In that region of overlap, when the two structures are combined, the index of refraction becomes negative and radiation can be transmitted through the material. The transmission curve for the combined structure has a peak between 11 and 11.5 GHz where the split-ring structure or wire structure alone gave no transmission.

Verification that we can realize the DNM designed in simulation enabled us to take the next step toward designing a structure with a uniquely customized dispersion curve.

4. Waveguide loaded with a dispersive, anisotropic medium

4.1. Continuous approximation of DNM

We investigated a waveguide loaded with a medium having double-negative properties within a certain frequency range. One motivation is a quest for control via the dispersion relation of the TM modes in a waveguide synchronous with a relativistic particle. It is desirable for accelerating structures to have a synchronous fundamental accelerating mode, while providing suppression of higher order modes that may disrupt a particle beam. Due to the heavy memory requirements of simulating a structure made up of very small, discrete elements, we began by looking at

the case of a waveguide loaded with a truly continuous double-negative medium. In such a structure higher order modes, in particular the dipole modes, are supported. However, an experimental structure is actually made up of discrete elements (DNM). The dipole mode is below the cutoff frequency of the empty waveguide, and it may be possible to suppress it. Research supporting this is ongoing and experimental tests are planned.

Since it is easier to load a rectangular waveguide with metamaterial than a cylindrical one, the following analysis is for a rectangular waveguide (along z) with an anisotropic (2D) medium inside. Analysis for a cylindrical waveguide is similar. Assume the following tensors for ε and μ for the medium inside the waveguide:

$$\hat{\varepsilon} = \begin{pmatrix} \varepsilon_\perp & 0 & 0 \\ 0 & \varepsilon_\perp & 0 \\ 0 & 0 & \varepsilon_\parallel \end{pmatrix}, \quad \hat{\mu} = \begin{pmatrix} \mu_\perp & 0 & 0 \\ 0 & \mu_\perp & 0 \\ 0 & 0 & \mu_\parallel \end{pmatrix}. \tag{3}$$

Here $\varepsilon_\perp$ has the form given by Eq. (1), $\mu_\perp$ has the form of Eq. (2), and the other components are positive constants. A metamaterial can realize the tensors given by Eq. (3). The dispersion relation for the TM modes of such a structure can be derived using standard methods [16,23,24]:

$$k_z = k_0 \sqrt{\varepsilon_\perp \mu_\perp \left(1 - \frac{\chi_x^2 - \chi_y^2}{\varepsilon_\parallel \mu_\perp k_0^2}\right)}. \tag{4}$$

Here $k_0 = \frac{\omega}{c}$, $\chi_x = \frac{\pi m}{a}$, $\chi_y = \frac{\pi n}{b}$, m, n are mode indices and a, b are dimensions of the waveguide. The analysis is done for the TM_{11} mode and is similar for any other mode. In order to have mode propagation to occur within a certain frequency band, $k_z(\omega)$ must be real, i.e., the expression under the root in Eq. (4) must be positive. This system has several characteristic frequencies: (1) cutoff frequency of the empty waveguide, ω_{cutoff} (for mode TM_{11}); (2) plasma frequency for the transverse permittivity, ω_p; and (3) resonant frequency for the transverse permeability, ω_{res}. These give the dispersion relation different characteristic frequency regions. The frequency dependence of $\mu_\perp, \varepsilon_\perp, \varepsilon_\parallel$ and the dispersion curve are plotted in Fig. 8 for the case when $\omega_{\text{cutoff}} < \omega_{\text{res}} < \omega_p$. The five characteristic frequency bands for this case are described below.

(I) This is the non-magnetic band similar to the one discussed in [16,25,26]. We see propagation below the cutoff frequency, similar to the non-dielectric example in Ref. [27]. The condition $\varepsilon_\perp \mu_\perp \leqslant 0$ is satisfied, but the frequency is below ω_{cutoff}, which allows $Re[k_z]$ to be non-zero.

(II) This region is characterized by negative ε and positive μ in the waveguide above the cutoff frequency. There is no propagation in this region accordingly (see Eq. (4)).

(III) In this region we observe classic left-handed behavior. The resonant permeability [6] causes the dispersion curve of the loaded waveguide to intersect the dispersion curve for highly relativistic electrons ($\omega/k = c = v_{\text{ph}}$). These curves are shown in Fig. 9 (bottom). The slope of the curve for the waveguide is negative signifying negative phase velocity. The intersection of the dispersion curves shows synchronism between the phase velocity of the backward waveguide mode and of the velocity of the electrons, so interaction is possible. Energy can be transferred from electrons to the waveguide mode, or vice versa. The dispersion curve of an empty waveguide (shown in Fig. 9 (top)) does not intersect that of an electron, so conventional waveguide accelerating structures often have irises or corrugations to synchronize the phase velocity of the guide to light speed.

(IV) In this region, we have $\varepsilon < 0$ and $0 < \mu < 1$. Nevertheless, propagation is possible, because low values of μ make an effective cutoff frequency ($\omega_{\text{cutoff}}^2/\mu$) higher than the frequency in this band. This band does not require negative values of μ to create a backward propagating mode. This quasi-non-magnetic band requires the condition $1 > \mu > 0$, which can be realized by natural diamagnetics.

(V) At the frequencies in this band, we have $\varepsilon > 0$ and $\mu > 0$. The behavior of the system resembles the behavior of an empty waveguide. There is no interaction between the relativistic electrons and the mode.

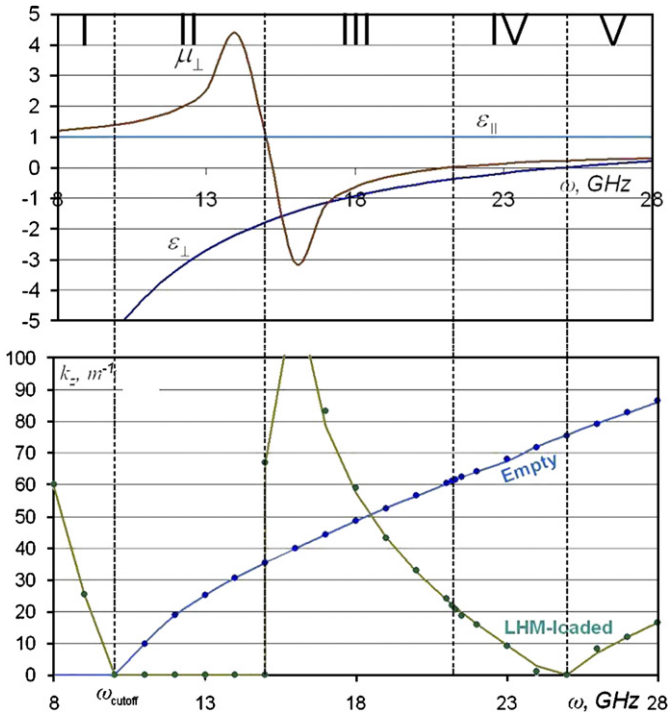

Fig. 8. The top plot in the figure shows the permeability μ of split-ring resonators and the permittivity of a wire array ε as a function of frequency. The bottom plot shows the dispersion curves for an empty waveguide and a waveguide loaded with the DNM (split rings and wire array). Five characteristic frequency regions for the loaded waveguide are indicated.

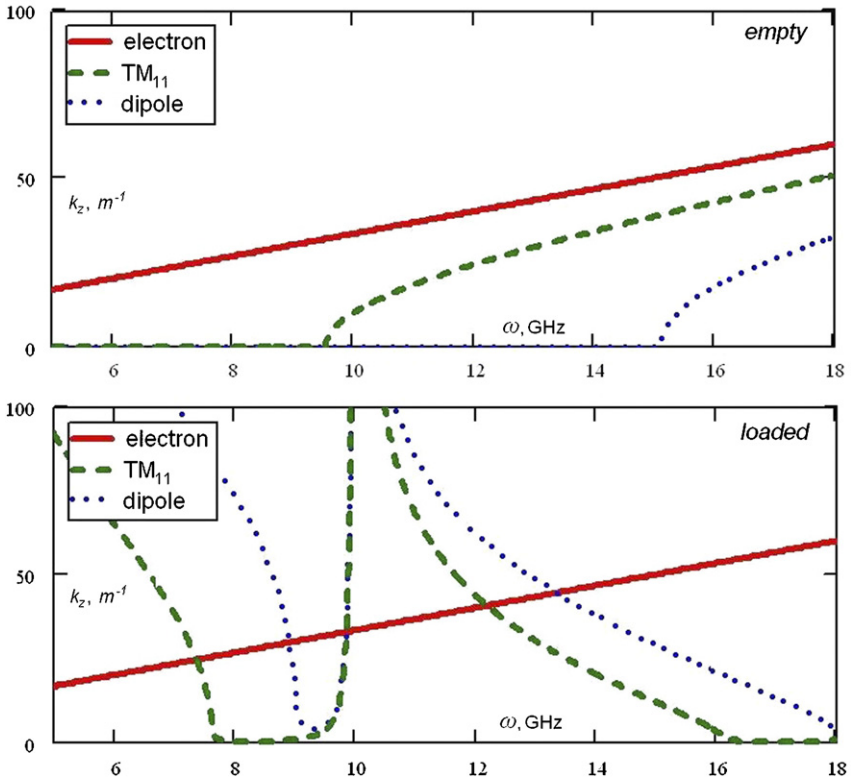

Fig. 9. The top figure shows the dispersion curves of the TM_{11} and dipole modes of an empty waveguide, along with the dispersion for a light speed electron. The bottom figure shows those same dispersion curves, but for a waveguide loaded with a DNM.

Dispersion analysis provides information about the frequency of synchronization with the particle for each mode and the group velocity for the excited mode. To obtain information on how much energy was transferred from the particle to each mode, one has to perform a wakefield calculation [28]. Calculation of Cherenkov radiation in double-negative media has also been presented in Refs. [29,30].

4.2. Discrete-element structures

Double-negative metamaterials are typically constructed of arrays of small, discrete elements and are not truly continuous media, despite the $\lambda \gg d$ condition. Preliminary work suggests that there are important practical implications to having a structure made up of discrete elements as opposed to a continuous medium. First, we discuss how construction details could have an impact on mode coupling in a waveguide structure. Second, we discuss the role the discrete nature of the material potentially plays in the suppression of higher order modes.

4.2.1. Construction

Due to the discrete nature of the metamaterial, we expect coupling between waveguide modes. This coupling is sensitive to the exact geometry of the integrated wire and SRR arrays. TM_{11} to TE_{10} mode coupling occurs due to scattering of radiation on the discrete metamaterial elements. In order to mitigate this potential problem, we moved away from the configuration shown in Fig. 10(a) to a more symmetrized geometry. The configuration of Fig. 10(a) has the wire array running along-side the SRRs. The second 2D configuration shown in Fig. 10(b) has the wires actually penetrating the centers of the loops comprising the SRRs. Boards with the metamaterial elements of this design are now in hand, and we are finishing the construction of the waveguide and coupler assembly for the next round of experimental tests. One of the goals of the upcoming experimental program is to observe excitation of the backward TM_{11} mode.

4.2.2. Potential for higher-order-mode suppression

It has been shown that region I of a dispersion relation such as that shown in Fig. 8 can support propagation; it is called a non-magnetic band [16,25,26]. In this band, backward propagation is realized due to the negative permittivity of the continuous medium operating in a region of the waveguide below the cutoff frequency. Operation below ω_{cutoff} provides a second negative under the root of the dispersion relation equation (4). The inside of a waveguide below cutoff frequency is a continuous medium that can be thought of as providing an effective negative permeability. However, it has been shown that there is no propagation through a wire array embedded in a continuous medium of negative μ [15]. Although the effective μ is continuous, the permittivity provided by the wire array is discrete, and in the spaces between the wires electromagnetic waves decay. Thus, we expect that a wire

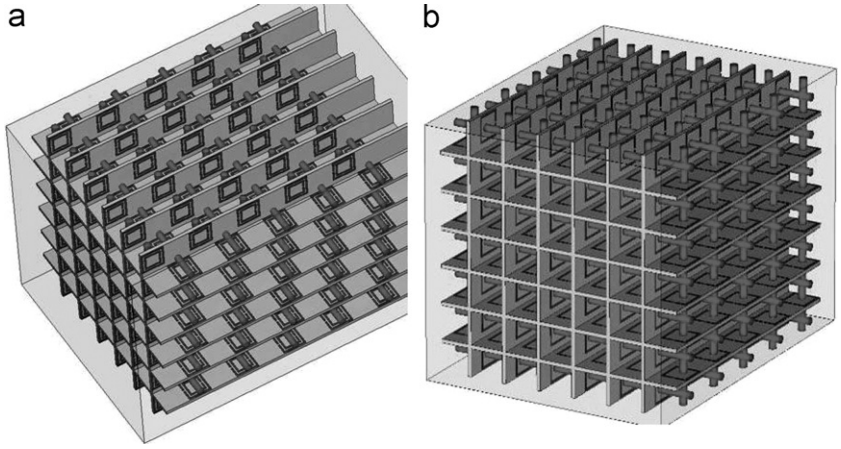

Fig. 10. Two-dimensional DNM array configurations: (a) wire array beside split rings; (b) wire array through split rings.

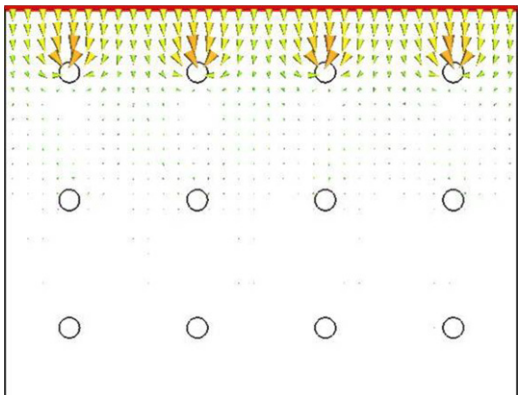

Fig. 11. Simulation of wire array in waveguide at frequency below ω_{cutoff} of the waveguide.

array in a waveguide below cutoff frequency will not support propagation in the non-magnetic band. We studied this case in simulations with a range of geometric parameters; one example of the results is shown in Fig. 11. The simulation is of a waveguide loaded with a wire array. The circles in Fig. 11 represent the wire cross-sections. The radiation is applied at the entrance of the guide, located at the top of the figure. The arrows show the calculated electric field, which decays before it can propagate to the other side (bottom of figure).

The failure of propagation in simulations for the case of the non-magnetic region (I) is, according to Ref. [15], due to the discrete permittivity presented by wires embedded in a continuous region of negative effective μ. Double-negative propagation in region III does not have this problem, because the metamaterial is double negative (supporting propagation) and the waveguide is operating above ω_{cutoff} (supporting propagation). It is these results that lead us to believe it may be possible to achieve dipole mode suppression in our discrete structure. The synchronous point for the dispersion relation of a relativistic electron and the dispersion curve of the dipole mode of the DNM loaded structure occurs below the cutoff frequency for the dipole mode (see Fig. 9). It is possible that the same behavior as in the non-magnetic region (I) will be observed for the discrete structure. The mode will be unable to exist due to the vacuum spaces between the planes of metamaterial arrays. Effort has begun on the simulation of a large scale discrete structure. So far, our simulation results are either for a continuous medium, or for discrete structures with only a limited number of elements. Preparations are in progress for experimental measurements using a waveguide loaded with DNM of our second design. These measurements will be a series of mode measurements, first exciting the waveguide and coupler assembly on the bench, and later driving it with a particle beam. We will be looking for excitation of the TM_{11} mode, and checking for the existence of any dipole mode excitation.

5. Conclusion

Exciting research on applications of double-negative metamaterials is being carried out world-wide, primarily by the optics and microwave engineering communities [1,2]. These materials are also potentially useful in the construction of particle accelerators, and research on the behavior of DNM loaded waveguides has been described. Simulations with continuous DNM materials identified several interesting frequency bands in the response of a loaded waveguide. Simulations and previous analytical work [15], however, indicate that there may be important differences between a truly continuous DNM and those manufactured using discrete elements. The most interesting of these is a potential mechanism for higher order mode suppression in a waveguide. Moreover, the unusual dispersion relation also points to potential particle detection applications. We have designed two different metamaterials. The first has been tested to verify that the behavior is that of a DNM at the design frequency. We are preparing to test the behavior of a waveguide loaded with DNM of our second design.

Acknowledgments

This work is supported by NSF Grant 0237162 and partially supported by the US DOE, Division of High Energy Physics, under Contract no. DE-AC02-06CH11357.

References

[1] C.M. Soukoulis, Science 315 (2007) 47.
[2] D.R. Smith, J.B. Pendry, M.C.K. Wiltshire, Science 305 (2004) 788.
[3] J.B. Pendry, Phys. Rev. Lett. 85 (2000) 3966.
[4] V.G. Veselago, Sov. Phys. USPEKI 10 (1968) 509.
[5] J.B. Pendry, A.J. Holden, W.J. Stewart, I. Youngs, Phys. Rev. Lett. 76 (1996) 4773.
[6] J.B. Pendry, A.J. Holden, D.J. Robbins, W.J. Stewart, IEEE Trans. Microwave Theory Tech. 47 (1999) 2075.
[7] D.R. Smith, et al., Phys. Rev. Lett. 84 (2000) 4184.
[8] F. Martin, F. Falcone, J. Bonache, R. Marquis, M. Sorolla, Appl. Phys. Lett. 83 (2003) 4652.
[9] F. Martin, F. Falcone, J. Bonache, T. Lopetegi, R. Marquis, M. Sorolla, IEEE Microwave Wireless Components Lett. 13 (2003) 511.
[10] E.I. Smirnova, A.S. Kesar, I. Mastovsky, M.A. Shapiro, R.J. Temkin, Phys. Rev. Lett. 95 (2005) 074801.
[11] G. Shvets, S. Kalmykov, AIP Conf. Proc. 737 (2004) 983.
[12] S. Antipov, W. Liu, W. Gai, J. Power, L. Spentzouris, AIP Conf. Proc. 877 (2006).
[13] S. Antipov, W. Liu, J. Power, L. Spentzouris, Design, Fabrication, and Testing of Left-Handed Metamaterial, Wakefield Notes at Argonne Wakefield Accelerator, ⟨http://www.hep.anl.gov/awa/wfnotes/wf229.pdf⟩.
[14] S. Antipov, W. Liu, J. Power, W. Gai, L. Spentzouris, PAC2007 Proceedings, submitted for publication.
[15] A.L. Pokrovsky, A.L. Efros, Phys. Rev. Lett. 89 (2002) 093901.
[16] V.A. Podolskiy, Ev.E. Narimanov, Phys. Rev. B 71 (2005) 201101(R).
[17] R.W. Ziolkovski, IEEE Trans. Antennas Propag. 51 (2003) 7.
[18] A.A. Zharov, I.V. Shadrivov, Y.S. Kivshar, Phys. Rev. Lett. 91 (2003) 037401.
[19] W. Rothman, IRE Trans. Antennas Propag. AP-9 (1962) 82.
[20] R. Shelby, D.R. Smith, S. Schultz, Science 292 (2001) 77.
[21] A. Houck, et al., Phys. Rev. Lett. 90 (2003) 137401.
[22] R.A. Shelby, D.R. Smith, S.C. Nemat-Nasser, S. Schultz, Appl. Phys. Lett. 78 (2001) 4.
[23] L.D. Landau, E.M. Lifshitz, L.P. Pitaevskii, Electrodynamics of Continuous Media, second ed., Butterworth, Oxford, UK, 1984.
[24] I.G. Kondrat'ev, A.I. Smirnov, Phys. Rev. Lett. 91 (2003) 249401.
[25] R. Wangberg, J. Elser, E.E. Narimanov, V.A. Podolskiy, J. Opt. Soc. Am. B 23 (3) (2006) 498.
[26] V.A. Podolskiy, L. Alekseyev, E.E. Narimanov, J. Mod. Opt. 52 (16) (2005) 2343.
[27] R. Marqués, et al., Phys. Rev. Lett. 89 (2002) 183901.
[28] A.V. Tyukhtin, S. Antipov, A.D. Kanareykin, P. Schoessow, PAC2007 Proceedings, submitted for publication.
[29] J. Lu, T.M. Grzegorczyk, Y. Zhang, J. Pacheco, B.I. Wu, J.A. Kong, M. Chen, Opt. Exp. 11 (2003) 723.
[30] Yu.O. Averkov, V.M. Yakovenko, Phys. Rev. B 72 (2005) 205110.